

Halftone modulation for embedding UV watermarks in color printed images

Vlado Kitanovski, Marius Pedersen

Color and Visual Computing Laboratory, Department of Computer Science
Norwegian University of Science and Technology

Gjøvik, Norway

{vlado.kitanovski, marius.pedersen}@ntnu.no

Abstract—A method for embedding ultraviolet (UV) responsive watermarks in CMY printed halftone images, named white modulation (WM), was proposed recently, which is based on the iterative color direct binary search (CDBS) halftoning framework. The CDBS-WM method embeds a visual watermark by modulating the local white paper coverage in order to create a differential response under UV illumination through the substrate fluorescence. In this paper, we present two main extensions of CDBS-WM. First, we propose a printer model suitable for UV watermark embedding in multi-channel printer scenarios – using four or more inks. Second, we propose an improved cost function that is minimized during the CDBS-based iterative embedding that takes into account the UV response of all primaries, as opposed to only the white primary in CDBS-WM. The proposed extensions increase the perceptual uniformity of the embedded UV watermark, as well as the UV watermark strength especially in certain image areas where the CDBS-WM failed to embed watermark.

Keywords—data hiding; UV watermark; security printing; halftoning; watermarking; color direct binary search

I. INTRODUCTION

Embedding hidden text or patterns in printed content is a common practice for increasing document security. The specific underlying technologies to achieve this include intaglio-printing, micro printing, infrared (IR) or ultraviolet (UV) security printing inks, just to name a few. Using special paper, inks, or printing technologies increases the cost, which is acceptable for printed documents of high value and long lifetime (e.g. banknotes or passports). When it comes to security features for documents with short lifetime and lower value, (e.g. tickets or vouchers) it is desirable that they can be produced using cheap and standard digital printing technologies, materials, and media.

From the wide range of watermarking techniques for printed content, relevant to this work are techniques for embedding visual watermarks using commonly available printers, inks and media, by exploiting illuminant-specific embedding and detection. These techniques embed visual watermark, such as text or logo, in the printed content so that the watermark is not perceptible under normal light (e.g. D50) but it can be easily revealed using a specific light source. Bala et al. proposed a method for embedding a binary visual watermark in color printed images, which uses sets of metameres and narrowband light sources [1]. The CMYK metameric pairs under D50 are chosen across

the whole gamut such that the pairs have maximally different response under the narrowband illumination. Their approach for obtaining and selecting suitable metameres is by varying the gray component removal strategy. Eschbach et al. proposed a method for embedding a visual watermark in laser-printed images, which exploits the infrared-reflecting property of paper substrates and the infrared-absorbing property of carbon black toners [2]. The binary visual watermark is embedded by utilizing metameric pairs with different amounts of the black colorant, which are highly distinctive and easily revealed under infrared illumination and using an infrared CCD sensor. Bala et al. proposed a method for embedding visual watermark, which exploits the fluorescent properties of Optical Brightener Agents (OBA) commonly present in paper substrates [3]. CMYK metameric pairs under D50 are obtained so that their fractional white paper coverages are different. The watermark is revealed under UV illumination because the printed areas with different amount of white paper have perceptually different response. Zhao and Wang proposed a similar method for embedding UV watermarks in natural color images [4]. Their method is using two different clustered-dot halftoning strategies according to the binary visual watermark: one for the background, which appears darker under UV due to the dot-off-dot distribution, and another halftoning strategy for the watermark, which appears brighter under UV due to the dot-on-dot distribution of printer dots (hence, higher fractional area of OBA-rich paper substrate).

In a recent work, we proposed the CDBS-WM method for UV-watermark embedding [5] that is based on the CDBS halftoning algorithm [6]. As in the previously published methods, the carrier of the hidden signal in CDBS-WM is the substrate fluorescence, which is modulated with the fractional coverage of white-paper area. The main difference from them is that instead of mapping (distinct under UV) metameric pairs, an iterative watermark embedding is used which takes into account the human visual system (HVS) properties - using an opponent-color space for color difference calculation and filtering with point-spread functions (PSFs). The CDBS-WM method also provides means to balance between properties like watermark perceptibility under normal light, watermark strength under UV light, or halftone texture. The evaluation using natural images showed that the method achieves low perceptibility of the embedded watermark under normal illumination, while achieving reasonably high UV-watermark strength.

In this paper, we propose an improved method for embedding UV watermarks in color printed images, which is also based on the CDBS halftoning framework. The two main contributions of this paper are: proposing a simple

printer model that is suitable for printers with four or more colorants, and proposing an improved halftone modulation method that embeds a visual UV watermark with higher halftone texture quality, higher perceptual uniformity, and higher watermark signal strength. The proposed printer model is described in section two, the proposed watermark embedding is described in section three, followed by experimental results and concluding remarks.

II. 2-BY-2 CENTERED PRINTER MODEL IN A MULTI-CHANNEL CDBS FRAMEWORK

The iterative CDBS halftoning algorithm minimizes a cost function that is the difference between the perceived original contone image and the perceived halftone image. The difference between these perceived images is expressed in an opponent color space suitable for filtering with PSFs that model the spatial characteristics of the HVS. The CDBS algorithm examines pre-defined trial changes of every single halftone pixel. These trial changes are efficiently evaluated in terms of their impact on the cost function. The change that causes the largest cost decrease is accepted and the process is repeated for every halftone pixel in several iterations until no halftone pixel change may further decrease the cost.

The halftone image is multidimensional – the number of dimensions is equal to the number of available printer colorants. In this work, the channels of the halftone image are binary – the halftone pixel value encodes whether a dot from each of the colorants is deposited or not. Thus, the value of each halftone pixel corresponds to a certain colorant combination, also referred as Neugebauer Primary (NP), which is deposited on the paper. Conversion of the halftone from colorant space to the (3D) opponent color space used in the CDBS is performed using a printer model. The printer model expresses the actual printed color at every halftone pixel location. The originally proposed CDBS CMY halftoning [6] uses the 2-by-2 centering printer model [7] that accounts for the nonlinear light-inks-paper interactions. The model assumes that the rendered image is of the same size as the halftone but with both 2D pixel coordinates shifted for half pixel, as shown in Figure 1. In that way, every pixel of the 2-by-2 rendered image is affected by four (2×2) halftone pixels, and every halftone pixel affects four pixels in the rendered image. The CDBS algorithm is actually minimizing the difference between the perceived original image and the perceived 2-by-2 rendered image. The nonlinear ink-paper interactions are in general not limited to the area of a 2-by-2 cell, so this mapping of a 2-by-2 cell to a rendered color by only taking into account the four halftone pixels may not be highly accurate. To tackle this, the 2-by-2 rendered colors within a predefined neighborhood can be further used in a Yule-Nielsen modified Neugebauer mixing model [8] to better predict the local rendered color [9,10]. However, such extension of the 2-by-2 model to a larger area would significantly increase the computational requirements (several orders of magnitude) of the iterative CDBS halftoning framework. This is the main reason why the 2-by-2 cells in the CDBS are mapped to a single color independently from the neighboring 2-by-2 cells; furthermore, this simple version of the 2-by-2 model is fairly accurate, especially for lower printing resolutions.

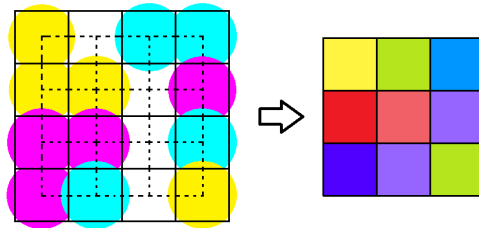


Figure 1. Color rendering using the 2-by-2 model. Left: Idealized circle-shaped colorant dots on a halftone grid (ideal printing grid), 2-by-2 rendering grid shown with dashed lines; Right: 2-by-2 rendered colors from the halftone, with bottom- and right-border pixels excluded.

The number of different colorant combinations in a 2-by-2 cell depends on the number of colorants, as well as the number of allowed halftone pixel values (nominally deposited NPs). If horizontal and vertical symmetry of the 2-by-2 cell is assumed, the number of different 2-by-2 rendered colors reduces to roughly 25%. In Table 1, we show examples for the number of 2-by-2 colors for different number of colorants and nominally deposited NPs.

From Table 1, it can be seen that the number of different 2-by-2 colors increases rapidly with the number of nominally deposited (allowed) NPs - whose maximum number is determined from the number of available colorants. In the CMY or CMY+K case, the number of 2-by-2 colors is reasonably low, so they can be measured macroscopically and stored in a lookup table (LUT) for use in the CDBS framework. However, in multi-channel scenarios, or even in the CMYK case where all of the 16 possible colorant combinations are allowed as nominal halftone pixel values, the number of measurements is too large and not practical. It is possible to use a combined model that measures a smaller set (5%-10%) in order to estimate parameters of a physical model that is used for prediction of all 2-by-2 colors [11]. Another related work states that printer models can be seen merely as computational mechanisms rather than attempts to model the physical phenomena of light-inks-paper interactions [12]. Inspired from that point of view, in this work we propose a simple computational model for estimating the whole set of 2-by-2 colors in multi-channel scenarios from a small training set. Based on the Yule-Nielsen modified Spectral Neugebauer model [8], we model the macroscopic reflectance $R(\lambda)$ of a periodical 2-by-2 pattern as:

$$R(\lambda) = \sum_{i=0}^{N-1} \left(a_i \cdot R_{NP}^{\frac{1}{n(wp,td)}}(\lambda) \right)^{n(wp,td)} \quad (1)$$

TABLE I. NUMBER OF 2-BY-2 COLORS RENDERED FROM A BINARY HALFTONE, DEPENDING ON AVAILABLE COLORANTS/NPS

	CMY	CMYK	CMYK	CMYKRGB	CMYKRGB
Number of nominally allowed NPs	8	9 (CMY + K)	16	64 (only 1, 2, and 3- colorant overprints)	128
2-by-2 colors	4096	6561	65536	16777216	268435456
2-by-2 colors with assumed symmetry	1072	1701	16576	4197376	67125184

In (1), a_i is physical coverage of the NP whose reflectance is $R_{NP}(\lambda)$, the Yule-Nielsen n -factor is made dependent on the number of white (no-colorant) pixels in the 2-by-2 cell, wp , and the total number of colorant drops in the 2-by-2 cell, td . The coverages a_i in (1) are obtained using the Demichel equations for all possible NPs [13]. For example, in the case of seven inks - CMYKRGB, the $N=2^7$ NP's effective coverages are calculated from the colorant physical coverages as follows:

$$\begin{aligned}
a_0 &= (1-c)(1-m)(1-y)(1-k)(1-r)(1-g)(1-b) \\
a_1 &= c(1-m)(1-y)(1-k)(1-r)(1-g)(1-b) \\
a_2 &= (1-c)m(1-y)(1-k)(1-r)(1-g)(1-b) \\
a_3 &= cm(1-y)(1-k)(1-r)(1-g)(1-b) \\
&\vdots \\
a_{127} &= cmykr gb
\end{aligned} \tag{2}$$

The colorant physical coverages c, m, y, k, r, g, b in (2) are obtained by fitting Yule-Nielsen model [14] using 2-by-2 single-colorant ramps.

Modelling the n -factor as in (1) is not uniform in terms of covering all of the 2-by-2 colors. For example, in the seven-ink CMYKRGB case, there are only seven 2-by-2 different colors made of three white pixels and one ink drop, there are 441 different 2-by-2 colors made of two white pixels and two ink drops at each of the two non-white pixels, and their number increases further with td . However, a single value of the n -factor is estimated for each valid (wp, td) combination. The reason for modelling the n -factor in this way is the observed variation of the optimal n value for different number of white pixels in the 2-by-2 cell as well as different amount of ink drops in the cell. From the equations (1-2) it can be recognized that this model not just assumes all symmetries in the 2-by-2 cell, but it also does not take into account the actual arrangement of colorant drops in the cell. The coverage of all possible NPs (2^k NPs for a binary halftone and k colorants) are calculated using (2) and used in the model (1) regardless of whether they are nominally printed at a halftone pixel location or not – all NPs in general occur due to mechanical dot gain and overlaps between neighboring dots.

The optimal value of the n -factor, $n(wp, td)$, for each (wp, td) combination is obtained by minimizing the CIEDE2000 (ΔE_{00}) color difference between the measured and predicted colors in the training set:

$$n(wp, td) = \arg \min_n (\Delta E_{00}(C_p, C_m)) \tag{3}$$

In (3), C_m is the CIELAB color of the measured training 2-by-2 samples, C_p is the predicted CIELAB color of the same sample using (1). Equation (3) is solved for each valid (wp, td) combination separately. In order to convert the colors from reflectance space to CIELAB tristimulus, we used D50 illuminant and color matching functions for the CIE1931 2° standard observer.

After obtaining the optimal $n(wp, td)$ values, the reflectances of all possible 2-by-2 combinations are calculated using (1) and converted to the YyCxCz (linearized CIELAB) opponent color space [15]. Finally, the calculated YyCxCz values are stored in a LUT for fast access during the CDBS halftoning or CDBS-like iterative watermark embedding.

III. MODULATION OF UV WATERMARK

In the CDBS-WM watermarking method [5], the UV watermark embedding is performed by modulating the white halftone pixels according to the binary visual watermark. This is achieved by extending the cost function that is minimized in CDBS with a binary watermark term that is dependent on the number of white halftone pixels. The embedding through the CDBS framework results in a halftone with two different regions, one with minimized white pixels and low fluorescent response (UV response), and another with maximized white pixels and higher UV response.

While the white primary (the fractional non-printed area) has strongest UV response, all other primaries also have a UV response that in general is non-zero. This fact is ignored in the CDBS-WM method, so in this work we propose an extension of the UV watermark embedding that takes into account the UV response of each printable 2-by-2 halftone cell. The cost function has the same form as in CDBS-WM i.e. it includes a term for the color difference between the perceived original image and the perceived 2-by-2 rendered watermarked halftone, and a watermark term:

$$E = \sum_i w_i \int |\tilde{e}_i(\mathbf{x})|^2 d\mathbf{x} + F_w[\mathbf{m}] \tag{4}$$

The first term in (4) is the weighted sum of color difference between the perceived original image and the perceived 2-by-2 rendered image. The watermark term, $F_w[\mathbf{m}]$, includes the binary watermark $W_M[\mathbf{m}]$, as well as a UV response term $U[h[\mathbf{m}]]$:

$$F_w[\mathbf{m}] = \alpha \cdot W_M[\mathbf{m}] \cdot U[h[\mathbf{m}]] \tag{5}$$

In (5), α is the overall watermark strength, the binary 2D spatial watermark $W_M[\mathbf{m}]$ has two levels, minus one or one, denoting the image areas where the UV response will be maximized or minimized, respectively. The UV response $U[h[\mathbf{m}]]$ depends on the halftone image $h[\mathbf{m}]$, or more precisely, it is the sum of the UV responses of the four 2-by-2 cells that include the 2D location \mathbf{m} . Accurate calculation of the radiance emanating from a printed substrate under UV light source is not possible when the UV illuminant is unknown – as in a real watermarking application. However, accurate calculation of the radiance is not essential for this particular watermarking scenario. What is sufficient is a quantity that is correlated with the pure fluorescent radiance from the print for a given UV light source. Such quantity can be estimated using the simple spectrophotometric approach [16]. If two spectrophotometric measurements of a given uniform sample, made without and with UV cutoff filter, are labelled as

$R_{UV}(\lambda)$ and $R_C(\lambda)$, the following quantity UV , named UV response, is correlated to the visible radiance emanating from the sample under the spectrophotometer's pure UV component:

$$UV = \int_{400nm}^{700nm} (R_{UV}(\lambda) - R_C(\lambda)) d\lambda \quad (6)$$

Making spectrophotometric measurements for all 2-by-2 combinations in order to obtain their UV response using (6) is not a viable option for multichannel scenarios due to the high number of 2-by-2 combinations (example given in Table 1). Therefore, an estimate of the UV response for each 2-by-2 cell, U , is obtained using the 2-by-2 predicted reflectances:

$$U = \int_{400nm}^{700nm} (R'_{UV}(\lambda) - R'_C(\lambda)) d\lambda \quad (7)$$

The predicted reflectances, $R'_{UV}(\lambda)$ and $R'_C(\lambda)$, are obtained from (1) using two different sets of NPs reflectances, $R_{NP,UV}(\lambda)$ and $R_{NP,C}(\lambda)$, measured without and with UV cutoff filter, respectively. An estimate of the UV response for all 2-by-2 cells is obtained using (7) and stored in a LUT for use during the iterative watermark embedding that minimizes the cost function in (4). More details about the actual minimization of a cost function of type (4) can be found in [5].

IV. RESULTS

In order to obtain the printer model in (1), we used a set of randomly generated 480 training 2-by-2 colors and 240 testing 2-by-2 colors that were sampled to cover all of the possible (wp, td) combinations. Additionally, the 2-by-2 single colorant ramps were printed to obtain the colorant physical coverages used in (2), and the full NPs were printed and measured both with and without UV cut filter to obtain the reflectances of the primaries $R_{NP,C}(\lambda)$ and $R_{NP,UV}(\lambda)$. The proposed printer model was generated for two different printers, CMYK Ricoh MP C6003 laser printer using the Multicopy Original A4 80gsm paper, and CMYKRGB HP Designjet Z3200 inkjet printer using the HP Premium Photo Matte 210gsm paper. The spectrophotometric measurements were made with the X-Rite i1Pro 2 spectrophotometer using the M1 and M2 measurement modes (without and with UV-cut filter). In the CMYK case, we used 15 NPs as nominal halftone pixel values, while in the CMYKRGB case we used 64 NPs – in both cases, they correspond to maximum three colorant overprints on the halftone grid. We estimated the parameters of the model in (1) and solved (3) using the training set and a brute-force search for global ΔE_{00} minimum per (wp, td) combination. For the CMYK laser printer, the optimal values of the n -factor for different number of white pixels in the 2-by-2 cell, wp , and different bands of the number of total colorant drops in the 2-by-2 cell, td , are shown in Figure 2a and Figure 2b. It can be seen that the optimal n -factor in general is increasing with

increasing the number of colorant drops and reducing the number of white pixels in the 2-by-2 cell. The same trend can be observed for the CMYKRGB inkjet case shown in Figure 2c and Figure 2d, even though the optimal n values are higher.

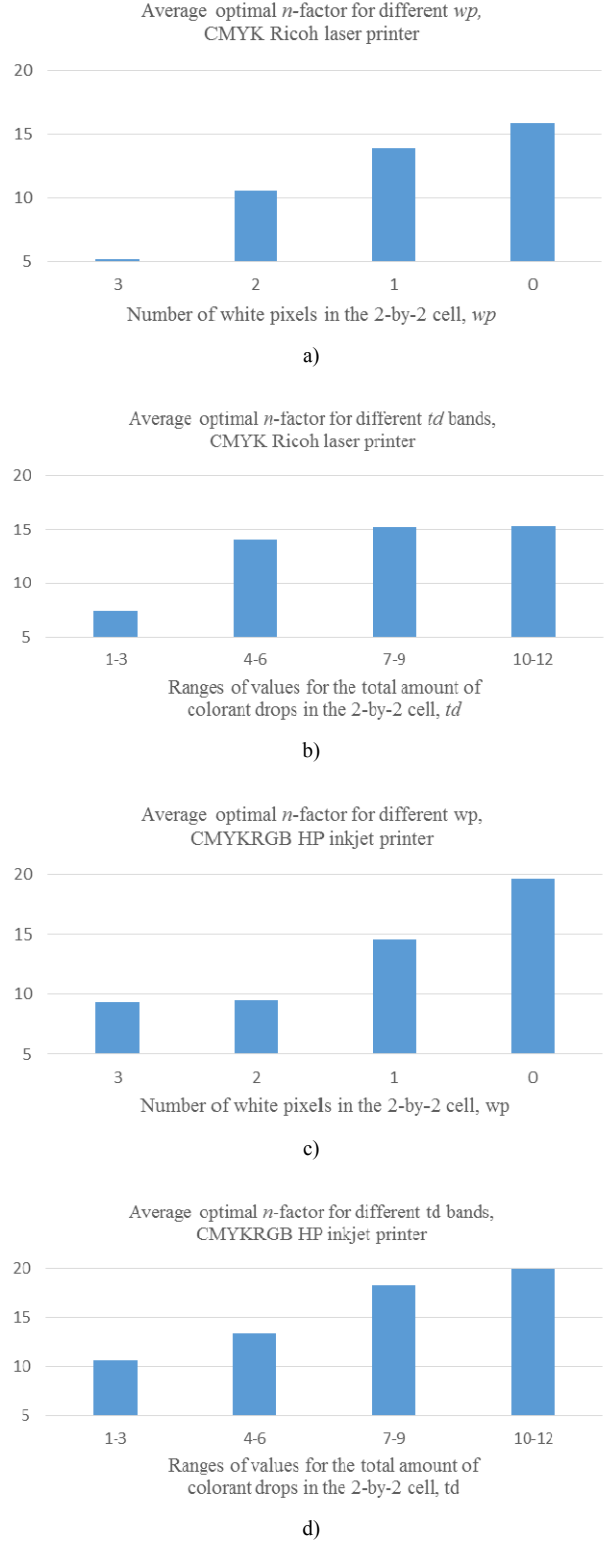


Figure 2. Dependency of the optimal values of the n -factor on the number of white pixels and total colorant drops in the 2-by-2 cell. a) and b) CMYK laser printer; c) and d) CMYKRGB inkjet printer.

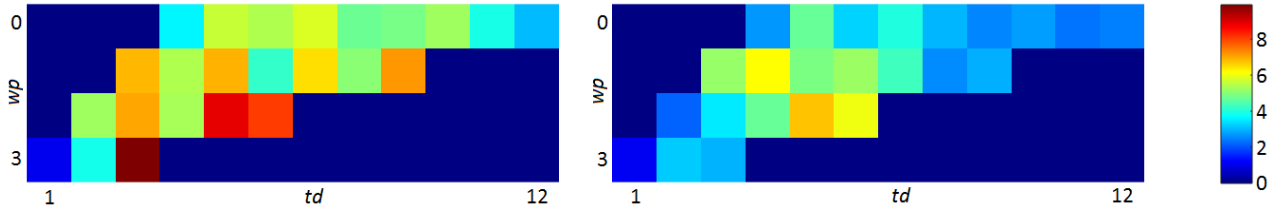


Figure 3. Average ΔE_{00} between predicted and measured testing samples, for different (wp, td) combinations, with a maximum of 3 colorants per halftone pixel. Left: CMYK laser printer; Right: CMYKRGB inkjet printer.

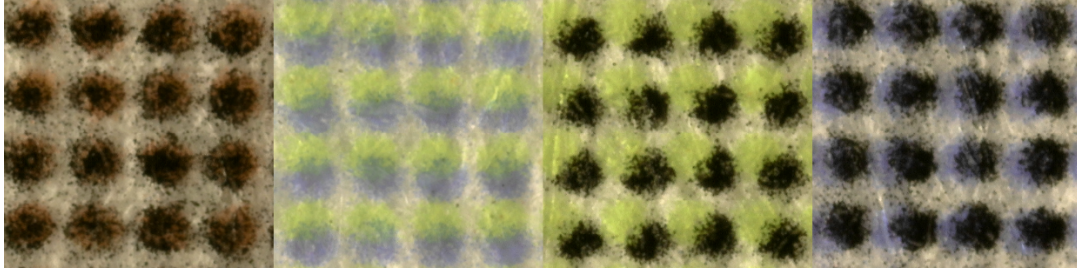


Figure 4. CMYK laser printer case, microscopic view of 2-by-2 cells with one non-white pixel made of two colorants. From left to right: magenta and black; cyan and yellow; yellow and black; cyan and black.

The average ΔE_{00} prediction errors on the testing set, for different wp and td values, are shown in Figure 3 for both printers. The overall average ΔE_{00} prediction error is 5.57 and 3.73, while the maximum error is 9.9 and 6.8, for the CMYK and CMYKRGB printer, respectively. In both cases, the prediction error is generally higher in the middle region of the wp - td span, and has a decreasing tendency towards the upper limit of colorant drops td . The prediction error is higher for the laser CMYK case than the inkjet CMYKRGB most likely due to the non-ideal square grid on which different colorant dots are deposited.

Even though the 2-by-2 modelling approach assumes ideally overlapping square grids for the different colorants, the actual locations of deposited dots is different among the CMYK laser printer colorants. Figure 4 shows four microscopic images of four periodic 2-by-2 cells with three white pixels ($wp=3$), and two colorant dots ($td=2$) at the non-white pixel location. It can be seen that only in first case the magenta and the black dot are well aligned as on the nominal halftone grid, while in the other three cases, the colorant dots are shifted from each other with only a partial overlap. These shifted printing grids of the different colorants, as well as the fact that the proposed 2-by-2 model does not account for the actual dots arrangement in the 2-by-2 cell, can be attributed to the increased prediction error in the laser CMYK case. In the CMYKRGB inkjet case, all of the colorant grids are very well aligned with each other, like in the left-most example shown in Figure 4.

As for the actual watermarking application, in this work, the UV watermark is embedded in a non-watermarked halftone as a post-halftoning step i.e. the watermark embedding is separated from the CDBS halftoning. The visual watermark that is embedded in all of the testing images is shown on Figure 5. We show examples using five natural color images of 800×800 that were printed at 300dpi. The images were watermarked using both the proposed watermarking method and the CDBS-WM method, using the proposed printer model in this paper. The color space used for both methods is YyCx Cz. The watermark strength, α , is constant for all

testing images but it is different between the two methods. The value of α was chosen so that the watermark distortion under normal light is somewhat equally perceptible for both methods. However, achieving equal perceptibility between the two methods is a difficult task because the embedded watermark using CDBS-WM is somewhat perceptually non-uniform. In the original work [5], CDBS-WM uses the CIELAB space instead of YyCx Cz to achieve higher perceptual uniformity of the watermark distortion, which comes at the price of grainier halftone texture and hence, lower image quality [5-6]. Figure 6 shows the CMYK watermarked images using both the CDBS-WM method (top) and the proposed method (bottom) captured under indoor office light. It can be observed that the proposed method achieves very low perceptibility and very good uniformity of the watermark embedding distortion under normal light – there are no image areas where the watermark can be easily spotted. This can be seen as an indirect verification for the suitability of the proposed printer model, as well as for the advantage brought by the cost function that takes into account the fluorescent response of all colorant combinations. On the other hand, the CDBS-WM watermarked images have parts where the watermark distortion is quite perceptible, for example, both the green and the dark parts of the flower image, the yellowish-neutral area under the beak of the second parrot image, or in the upper parts of the building façade in the third image. Using only the white primary in CDBS-WM can be seen as a more aggressive embedding approach that may cause visible distortions in certain image parts.



Figure 5. The used binary visual watermark $W_{vis}[\mathbf{m}]$.



Figure 6. CMYK printed watermarked images under office light, using CDBS-WM (top row) and the proposed method (bottom row). Best viewed in the electronic version of this paper.

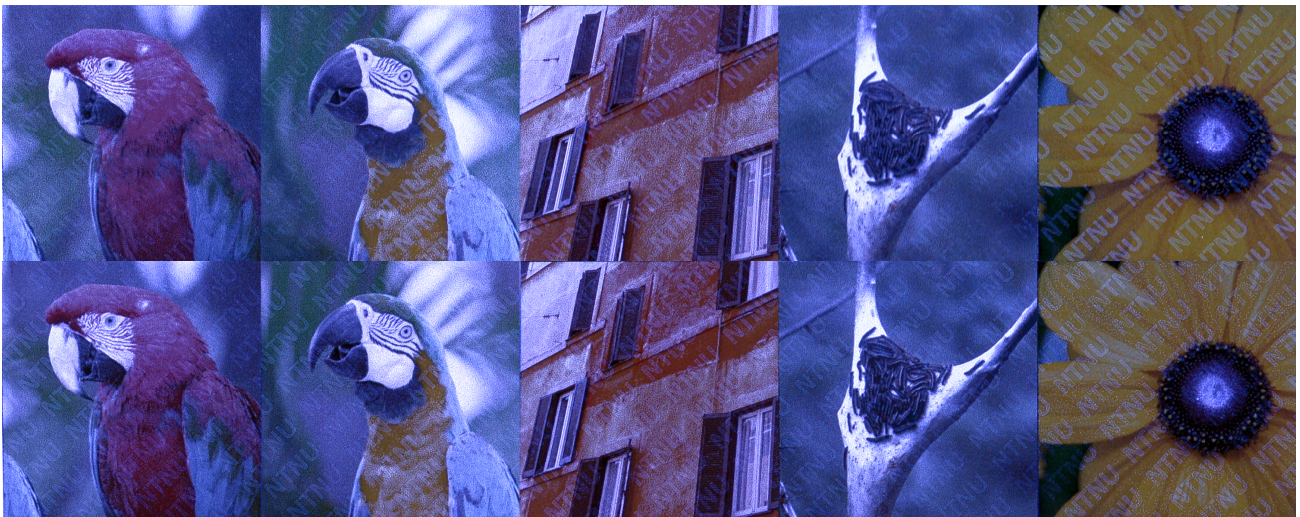


Figure 7. CMYK printed watermarked images under both office and UV light, obtained using CDBS-WM (top row) and the proposed method (bottom row). Best viewed in the electronic version of this paper.

Another suspected reason for the poorer performance of the CDBS-WM method is the small inaccuracy of the proposed 2-by-2 printer model - it is computational and not fully measurement-based as in the original CMY-based CDBS-WM work [5]. The same images under office light with added UV light are shown in Figure 7. It can be seen that the UV watermark strength for the proposed method is more uniform than for the CDBS-WM method. The proposed method also achieves higher UV watermark strength and higher contrast of the watermark, except for the flower image that has a lot of amounts of saturated yellow. The large UV watermark strength variations for the CDBS-WM, as mentioned before, can be partially tackled by using CIELAB in the whole framework. However, the watermark embedding using the proposed method seems to be more balanced and the convergence to the watermarked halftone perceptually more robust to printer model inaccuracy. The proposed method achieves high UV watermark strength in certain parts of the images where the CDBS-WM did not achieve (together with preserving watermark imperceptibility under normal light) even using different parameter settings, such as the upper

right corner of the first image, the most right part of the second image, the upper left corner of the third image. Or the central darker part of the flower image. This is a result of the added flexibility to use all of the primaries to modulate the fluorescent response

The same images watermarked with both methods using the proposed printer model for the CMYKRGB inkjet printer are given in Figure 8 and Figure 9, as seen under office light and office light with added UV, respectively. Similar as in the CMYK case, the proposed method achieves stronger and rather uniform UV watermark response, with higher contrast, except for the areas with dominant yellow colorant. The watermark distortion under normal light is also more perceptually uniform across different parts of the gamut, even though this difference is smaller when compared to the CMYK case. Figure 10 shows selected cropped and zoomed portions of Figures 6-9 that show the improvement of the proposed method over CDBS-WM in terms of watermark imperceptibility and UV signal strength. Figures 6-10 are best viewed at full or double scale in the electronic version of this paper.



Figure 8. CMYKRGB printed watermarked images under office light, using CDBS-WM (top row) and the proposed method (bottom row). Best viewed in the electronic version of this paper.



Figure 9. CMYKRGB printed watermarked images under both office and UV light, obtained using CDBS-WM (top row) and the proposed method (bottom row). Best viewed in the electronic version of this paper.

V. CONCLUSION

In this paper, we propose a halftone modulation method for embedding visual watermarks in color printed images. The embedded watermark is hardly perceptible under normal light, but it is easily revealed using a UV light source due to the paper fluorescent whitening agents. The watermark embedding uses a modified 2-by-2 printer model, and it takes into account the UV fluorescent response of all deposited primaries. The improvement of the proposed method over our previous white modulation method [5] can be summarized in few points that are, however, interconnected between each other. First, the proposed printer model is suitable for use by printers with four or more inks. Second, the UV characterization of all deposited colorant combinations makes the watermark embedding distortion perceptually more uniform, and due to the use of the $YyCx Cz$ color space, the final halftone texture is smoother resulting in higher quality of the printed image. At last, the UV response of the embedded watermark is in general stronger, with more consistent strength, and the watermark itself is successfully embedded in larger parts of the image gamut.

REFERENCES

- [1] R. Bala, K. M. Braun, and R. P. Loce, "Watermark Encoding and Detection using Narrowband Illumination", Proc. 17th Color Imaging Conference, pp. 139-142, Albuquerque, NM, Nov. 2009.
- [2] R. Eschbach, R. Bala, M. Maltz, and I. Zhao, "Creating Variable Data Infrared Signals for Security Applications", SPIE Proceedings: Color Imaging XIII: Processing, Hardcopy, and Applications, R. Eschbach et al. Eds., Vol. 6807, pp. 72411E-72411E-9, San Jose, CA, Jan 2008.
- [3] R. Bala, R. Eschbach, and Y. Zhao, "Substrate Fluorescence: Bane or Boon?", Proc. 15th Color and Imaging Conference, pp. 12-17, Albuquerque, NM, Nov. 2007.
- [4] Y. Zhao and S. Wang, "UV fluorescence encoded image using two halftoning strategies", SPIE Proceedings: Color Imaging XVI: Displaying, Processing, Hardcopy, and Applications, R. Eschbach et al. Eds., Vol. 7866, pp. 78661D-78661D-8, San Francisco, CA, Jan. 2011.
- [5] V. Kitanovski, R. Eschbach, M. Pedersen, J. Y. Hardeberg, "Data Hiding by White Modulation in Color Direct Binary Search Halftones", Journal of Imaging Science and Technology, Vol 61, No. 4, 2017.
- [6] A. U. Agar, and J. P. Allebach, "Model-Based Color Halftoning Using Direct Binary Search", IEEE Transactions on Image Processing, Vol.14, No.12, pp. 1945- 1959, Dec. 2005.

- [7] S. G. Wang, "Algorithm-independent color calibration for digital halftoning", Proc. Fourth Color Imaging Conference, pp. 75-78, Nov. 1996.
- [8] J. A. C. Yule and W. J. Nielsen, "The penetration of light into paper and its effect on halftone reproduction", Proc. TAGA, 3, 65-76, 1951.
- [9] S. Wang, "Two-by-Two Centering Printer Model with Yule-Nielsen Equation", Proc. International Conference on Digital Printing Technologies 1998, pp. 302-305, 1998.
- [10] M. Hebert, R. D. Hersch, "Review of spectral reflectance models for halftone prints: principles, calibration, and prediction accuracy", Color Research and Application, Vol. 40, No. 4, pp. 383-397, 2015.
- [11] V. Babaei, R. Rossier, and R. D. Hersch. "Reducing the number of calibration patterns for the two-by-two dot centering model", SPIE Proceedings: Color Imaging XVII: Displaying, Processing, Hardcopy, and Applications, R. Eschbach et al. Eds., Vol. 8292, pp. 829208-829208-9, San Francisco, CA, Jan. 2012.
- [12] P. Morovic, J. Morovic, X. Farina, P. Gasparin, M. Encrenaz, and J. Arnabat, "Spectral and color prediction for arbitrary halftone patterns: a drop-by-drop, WYSIWYG, "ink on display" print preview", Proc. 23rd Color Imaging Conference, pp. 2-6(5), Oct. 2015.
- [13] E. Demichel, in Procédé, 26, 17-21 and 26-27, 1924.
- [14] J. A. C. Yule and G. G. Field, Principles of Color Reproduction, GAFT Press, Pittsburgh, 215, 2000.
- [15] T. J. Flohr, B. W. Kolpatzik, R. Balasubramanian, D. A. Carrara, C. A. Bouman, and J. P. Allebach, "Model based color image quantization", SPIE Proceedings: Human Vision, Visual Processing, and Digital Display IV, J. P. Allebach et al. Eds., Vol. 1913, pp. 270-281, San Jose, US, Jan. 1993.
- [16] Y. Zhao and R. Bala, "Printer Characterization for UV Encryption Applications", Proc. 16th Color Imaging Conference, pp. 79-83, Nov. 2008.

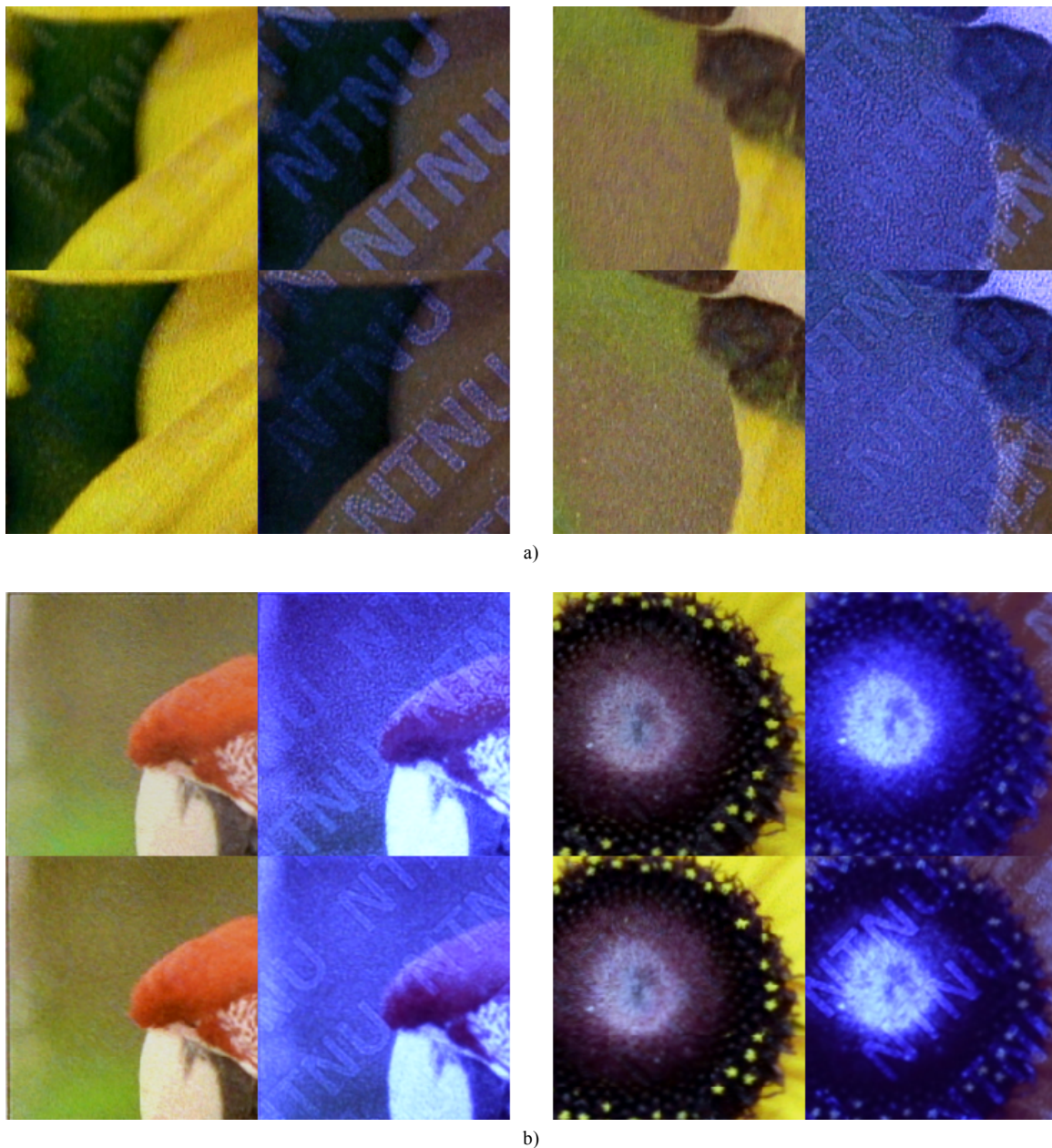


Figure 10. Selected cropped and zoomed portions from Figures 6-9. CDBS-WM (top pairs) compared to the proposed method (bottom pairs).
 a) CMYK laser-printed images; b) CMYKRGB inkjet-printed images. Best viewed in the electronic version of this paper.